Bioconjugate Chemistry

Article

pubs.acs.org/bc

Potent Retro-Inverso D-Peptide for Simultaneous Targeting of Angiogenic Blood Vasculature and Tumor Cells

Ying Li,[†] Yang Lei,[†] Ernst Wagner,[†] Cao Xie,[†] Weiyue Lu,[†] Jianhua Zhu,[‡] Jie Shen,[†] Jing Wang,[†] and Min Liu*[,†]

[†]Key Laboratory of Smart Drug Delivery, Ministry of Education and PLA, Department of Pharmaceutics, and [‡]Department of Radiopharmacy, School of Pharmacy, Fudan University, 826 Zhangheng Road, Shanghai 201203, P.R. China

Supporting Information

ABSTRACT: The application of tumor targeting ligands for the treatment of cancer holds the promise of enhanced efficacy and reduced toxicity. L-SP5 ($_{L}$(SVSVGMKPSPRP)) is a peptide that recognizes tumor neovasculature but not normal blood vessels (Lee et al., *Cancer Res.* **2007**, *67*, 10958−65). The current report presents the design and application of D-SP5 ($_{D}$(PRPSPKMGVSVS)), a novel retro-inverso analogue of L-SP5. Peptides D-SP5 and parental L-SP5 are shown to compete for the same target sites of a yet unknown cellular target and possess a dual-targeting bioactivity for both activated endothelial cells (HUVEC) and several tumor cell lines. Cellular uptake experiments showed superior in vitro targeting abilities of D-SP5 compared with L-SP5, such as enhanced internalization into stimulated HUVEC or KB, U87, and SGC tumor cells. A radioligand receptor binding assay revealed a higher cell affinity of D-SP5 in all tested cell lines, with K_d values for D-SP5 about 2-fold lower than for L-SP5. An up to 3-fold higher maximum binding capacity (B_{max}) to cells of D-SP5 was noted. Fluorescein-labeled D-SP5 upon intravenous administration displayed strong association with tumor endothelium. D-SP5-conjugated PEG-DSPE micelles displayed enhanced tumor homing (evidenced by near-infrared in vivo imaging). When loaded with doxorubicin, D-SP5 micelles could markedly suppress tumor growth with higher efficacy than L-SP5 micelles both in vitro and in vivo in KB tumor xenografts. In summary, the data demonstrate that D-SP5 displays higher binding affinities toward tumor endothelium as well as tumor cells and enhanced tumor targeting capability in vitro and in vivo.

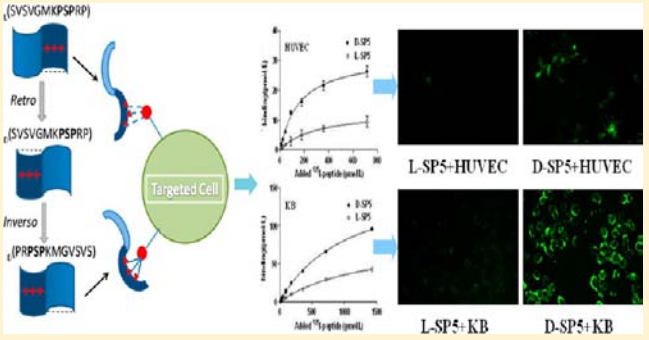

INTRODUCTION

One of the key issues for successful cancer treatment is to deliver effective doses of chemotherapeutic agents or antibodies into the tumors while minimizing the adverse effects to healthy tissues.[1,2] The interstitial fluid pressure in the solid tumors is higher than in normal organs, which may result in failure for standard drugs to accumulate in the tumor target regions.[3−5] To overcome this problem, several approaches could be considered. Compared with normal cells, most tumors have unique growth characteristics. In order to meet the great demand of such growth, new blood vessels are formed without the lining of functional pericytes around the endothelial cells. Thus, these blood vessels are usually leaky, with fenestrations of an average pore size of 100−600 nm, depending on the type of tumor. In addition, tumor tissues are short of lymphatic vessels, which, together with the leakiness of the vasculature, allows nanoparticles to diffuse into and be entrapped within the tumors. This passive tumor accumulation is also referred to as the enhanced permeability and retention (EPR) effect.[6−8] Self-assembled polymeric micelles are promising drug carriers with narrow distribution of size (1−100 nm) for anticancer agents.[9,10] Drugs can be embedded within the hydrophobic core of polymeric micelles, which greatly increase both solubility and stability of drugs. Poly(ethylene glycol)-phospholipid based micelles usually have prolonged in vivo circulation times necessary for drug tumor accumulation.[11]

Nevertheless, besides the passive targeting by EPR effect, several specific endothelial surface markers are expressed on tumor vasculature,[12−15] which are barely detectable in normal vessels and organs.[16−18] Therefore, finding the corresponding target ligands that specifically bind to the tumor microenvironment (i.e., tumor vessels and tumor cells) presents an important task in anticancer therapy. Use of polymeric micelles conjugated with such target ligands makes it possible to deliver encapsulated chemotherapeutic drugs into cells through receptor-mediated endocytosis.[19−22]

Retro-inverso peptide analogues, also called retro-all-D or retroenantio peptide analogues, are obtained through assembling amino acid residues in the reverse order of the parent peptide sequence and replacing L- with D-amino acids. Theoretically, retro-inverso peptides, unless fixed in special secondary structures, present an orientation of their side chains

Received: September 24, 2012
Revised: December 9, 2012
Published: December 17, 2012

dx.doi.org/10.1021/bc300537z | *Bioconjugate Chem.* 2013, 24, 133−143

very similar to that of the original structure.[23,24] Such peptides are resistant to protease degradation, have modified antigenicity, and may have equal or even higher bioactivities compared with the parent L-peptides.[25−28]

L-SP5, previously reported as SP5−52, a linear peptide which contains twelve amino acids, was discovered by an in vivo phage display screen to recognize blood vessels in SCID mice bearing solid tumors.[29] In the current study, we synthesized the retro-inverso form of L-SP5, named D-SP5 ($_D$(PRPSPKMGVSVS)), and investigated its tumor targeting property. Through cellular uptake experiments and radioligand receptor binding assays (RBA), D-SP5 was found to possess dual-targeting abilities to both tumor neovasculature and tumor cells. Moreover, it exhibited surprisingly enhanced binding affinities compared with L-SP5. Also, D-SP5 targeted micelles (D-SP5-micelles/Dox), consisting of D-SP5 conjugated poly(ethylene glycol) phosphatidyl ethanolamine (D-SP5-PEG-DSPE), methoxy poly(ethylene glycol) phosphatidyl ethanolamine (mPEG-DSPE), and doxorubicin (Dox), exhibited enhanced tumor cytotoxic efficacy compared with L-SP5 conjugated micelles (L-SP5-micelles/Dox), nontargeted micelles (M-micelles/Dox) or free Dox, against KB cells both in vitro and in vivo. These results indicate that D-SP5 peptide may have great potential as a drug targeting agent in cancer therapy.

MATERIALS AND METHODS

Materials. Boc-amino acids were purchased from GL Biochem Ltd. (Shanghai, China). Peptide synthetic resin was from Fluka (Switzerland). *O*-Benzotriazole-*N*,*N*,*N*′,*N*′-tetramethyl-uronium-hexafluorophosphate (HBTU) and *N*,*N*-diisopropylethylamine (DIPEA) were obtained from American Bioanalytical (USA). Fluorescein-5-maleimide (MAL-FITC) was purchased from Fanbo Biochemicals (Beijing, China). Mal-PEG-DSPE was purchased from Laysan Bio Co., USA. Sephadex G50 was purchased from Sigma (St. Louis, USA). DiR (1,1′-dioctadecyl-3,3,3′,3′-tetramethyl indotricarbocyanine iodide) was from Invitrogen, USA. mPEG2000-DSPE was purchased from Lipoid GmbH (Ludwigshafen, Germany). Dulbecco's modified Eagle medium (DMEM) and fetal bovine serum (FBS) were purchased from Gibco Co. (USA). Rat antimouse CD31 was from Abcam (USA). Goat antirat IgG conjugated to rhodamine was purchased from Santa Cruz Biotechnology Inc. (USA). DAPI was supplied by Roche, Switzerland. Tissue-tek OCT compound was supplied by Sakura Finetek USA Inc. Vascular endothelial growth factor (VEGF) and basic fibroblast growth factor (bFGF) were obtained from Sino Biological Inc. (Beijing, China). Mouse serum was purchased from GuangZhou Jianlun Biology Technology Co.(Guangzhou, China). Dox·HCl was purchased from Zhejiang Haizheng Co. (Zhejiang, China).

HUVEC (human umbilical vein endothelial cells), KB (human oral epidermoid carcinoma cells), U87 (human glioblastoma cells), SGC (human gastric carcinoma cells), and L02 (normal human hepatocytes), obtained from Shanghai Institute of Cell Biology (Shanghai, China), were cultured in DMEM containing 10% FBS, 100 U/mL penicillin, and 100 μg/mL streptomycin under a humidified atmosphere of 5% CO_2/air at 37 °C.

Male BALB/c nude mice of 4−6 weeks of age were obtained from Shanghai SLAC Laboratory Animal Co., Ltd. (Shanghai, China) and kept under SPF conditions. All animal experiments were evaluated and approved by the Ethics Committee of Fudan University.

Synthesis of Peptides and Derivatives. D-SP5 ($_D$(PRPSPKMGVSVS)), L-SP5 ($_L$(SVSVGMKPSPRP)), and control peptide ($_D$(PSMVKGSRVPPS)) were synthesized using Boc-protected amino acids on solid-phase PAM resins using standard coupling procedures. HBTU/DIPEA was used as coupling reagent. In order to label with fluorescein and radionuclide, cysteine and tyrosine derivatives of the above peptides were synthesized; peptide sequences were shown in Table 1. The peptides were purified using a reverse-phase HPLC (RP-HPLC) and the sequences were confirmed using a mass spectrometry method (ESI-MS, Figure S1).

Table 1. List of Synthesized Peptide Sequences[a]

D-peptide	sequence	L-peptide	sequence
D-SP5	$_D$(PR**PSP**KMGVSVS)	L-SP5	$_L$(SVSVGMK**PSP**RP)
D-SP5-Cys	$_D$(PR**PSP**KMGVSVS<u>C</u>)	L-SP5-Cys	$_L$(<u>C</u>SVSVGMK**PSP**RP)
D-SP5-Tyr	$_D$(PR**PSP**KMGVSVS<u>Y</u>)	L-SP5-Tyr	$_L$(<u>Y</u>SVSVGMK**PSP**RP)
Control peptide	$_D$(PSMVKGSRVPPS)		

[a]Amino acid residue **PSP** refers to the potential crucial motif for tumor targeting ability; and <u>C</u> or <u>Y</u> was labeled for further modification (on the opposite side to expose PSP motif).

Synthesis of FITC-Labeled D-SP5. To prepare fluorescein-labeled peptides, 5 mg peptide-Cys derivative was dissolved in 1 mL of PBS (0.05 mol/L, pH 7.4). A 1.2× molar excess of Mal-FITC was dissolved into the above solution and stirred for 2 h. Then, the mixture was purified via an HPLC system (Waters 600E, USA) on a Symmetry 300 Å C-18 reversed column (300 mm × 19 mm, Waters Co.) using a gradient method. The mobile phase A consisted of distilled H_2O with 0.1% (v/v) trifluoroacetic acid (TFA). The mobile B consisted of acetonitrile with 0.1% (v/v) TFA. The elution gradient was 60 min linear gradient from 5% B to 65% B at a flow rate of 10 mL/min. The product was collected and lyophilized for further use.

Peptide Iodination. Peptides were iodinated following an Iodogen method as reported.[30] In brief, a 1.5 mL polypropylene tube was coated with 10 μg of iodogen in $CHCl_3$ (0.2 mg/mL) and air-dried. Two micrograms D-SP5-Tyr or L-SP5-Tyr was mixed with 1.3 mCi $Na^{125}I$ in 30 μL of 0.2 mol/L HEPES buffer (pH 7.2), respectively. The mixture was allowed to react for 5 min under stirring at 25 °C and was then fractionated on a 1 × 10 cm Sephadex G-10 column eluted with 50 mmol/L HEPES buffer (pH 7.2). ^{125}I-radiolabeled D-SP5-Tyr and L-SP5-Tyr were collected and stored at 4 °C. Radiochemical purity of these peptides was determined on a YMC C-18 reversed-phase column using TFA/acetonitrile as a mobile phase via HPLC system (Agilent 1100 Series, Palo Alto, USA). Specific radioactivity was typically 600 mCi/μg.

Targeting Property of Retro-Inverso Peptide D-SP5. *In Vitro Cellular Uptake of FITC-D-SP5.* In order to investigate the affinity of D-SP5 to neovasculature endothelia, HUVEC cells were transferred to 33 mm culture dishes at 2 × 10^5 cells per dish. The cells were pretreated with 20 ng/mL of VEGF and 2 ng/mL of bFGF for 48 h to stimulate HUVEC. The VEGF-stimulated HUVEC were incubated with 0.5 μmol/L of FITC-labeled peptides (FITC-D-SP5, FITC-L-SP5, and FITC-control peptide) for 4 h at 37 °C, respectively. Cells were washed three times with PBS and directly observed under a

dx.doi.org/10.1021/bc300537z | Bioconjugate Chem. 2013, 24, 133−143

fluorescence microscope (DMI4000 B, LEICA, Germany). To investigate whether the D-SP5 and L-SP5 can bind with the stimulated-HUVEC at a same binding site, 1 mmol/L unlabeled L-SP5 was used to compete with FITC-D-SP5. An equal molar concentration of FITC-labeled control peptide was used as a negative control. The cellular uptake of FITC-labeled peptides (FITC-D-SP5, FITC-L-SP5, and FITC-control peptide) by KB, U87, and SGC was also studied following the same procedure described above.

Radioligand Binding Assay of Receptors. Radioligand binding assays on different cell lines were performed to further compare the binding affinities of ^{125}I-labled D-SP5 and L-SP5 peptide (^{125}I-D-SP5 and ^{125}I-L-SP5) . Briefly, the stimulated-HUVEC and the other three human tumor cells (KB, U87, and SGC) were incubated with 0.01−1.5 nmol/L ^{125}I-D-SP5 and ^{125}I-L-SP5, respectively. After incubation for 4 h at 4 °C, the cells were collected by centrifugation at 1000*g* for 5 min at 4 °C. The collected cells were washed with 1 mL of ice-cold PBS buffer and centrifuged. Radioactivity of these samples was measured via a gamma counter (SN-682, Rihuan, China). Following the same procedure, the cells were treated with unlabeled peptide in 200-fold molar excess to determine nonspecific binding for different cell lines. Specific binding was calculated by subtracting the nonspecific binding from the total binding. All assays were performed in triplicate. Dissociation constant (K_d) and maximum binding capacities (B_{max}) were determined by Scatchard analysis of saturation curves using *GraphPad Prism*.

Tissue Preparation and Immunohistochemical Analysis. Immunofluorescence study was carried out to investigate targeting mechanism of peptide D-SP5. KB cells (1.2×10^6 cells per mouse) were subcutaneously inoculated in the right flank of nude mice. FITC-labeled D-SP5 was intravenously injected 15 days post inoculation when the mice had visible tumors of approximately 8−10 mm in diameter. At 2 h following the injection, the mice were sacrificed for the tumors. FITC-labeled L-SP5 was produced by the same procedures and used as contrast. The tumors were excised and fixed with 4% paraformaldehyde for 12 h. Then, the fixed tumors were soaked in 30% sucrose in PBS overnight, frozen in OCT embedding medium, and then snap-frozen in liquid nitrogen. The tumor tissues were cut into 10-μm-thick slices using a Cryostat (MICROM International GmbH, Walldorf, Germany). Sections of the tumor tissues were fixed in ice-cold acetone for 10 min at 4 °C and washed with PBS, and blocked with bovine serum albumin (BSA) for 1 h. For labeling blood endothelial cells, sections were incubated with rat antip-mouse CD31 (1:10, v/v) for 1 h, followed by detection with goat anti-rat IgG conjugated to Rhodamine (1:100, v/v). Slides were treated with DAPI for nuclear counterstaining, and visualized using a fluorescent microscope (DMI4000 B, LEICA, Germany).

Ex Vivo Stability Studies of D-SP5 and L-SP5 Peptides in Diluted Mouse Serum. The stabilities of D-SP5 and L-SP5 peptides were investigated in commercially available pooled mouse serum diluted to 50% with distilled water. 1.5 mg peptide was dissolved in 2 mL pooled sterile mouse serum. After incubation periods of 0, 5, 10, 15, and 30 min, and 1, 1.5, 2, 4, 6, 8, and 10 h at 37 °C, 100 μL serum medium was taken out and added with 500 μL methanol to precipitate the serum proteins. Then, the mixture was stored at 4 °C for 20 min, and centrifuged at 13 000 rpm for 10 min. The remaining amounts of peptides were quantified by using reverse-phase HPLC (The elution gradient was 30 min linear gradient from 5% acetonitrile to 65% acetonitrile at a flow rate of 0.7 mL/min). All experiments were carried out three times.

Synthesis and Characterization of D-SP5-PEG-DSPE. D-SP5-PEG-DSPE was synthesized by reacting 2.9 mg D-SP5-Cys with an equimolar quantity of 8.26 mg Mal-PEG-DPSE in 1 mL PBS buffer (pH 7.0, 1/15M). The reaction mixture was stirred for 1 h at room temperature. The peptide was covalently linked to the maleimide group of Mal-PEG-DSPE via the thiol of the unprotected cysteine, to yield L-SP5-PEG-DSPE and D-SP5-PEG-DSPE. The reaction mixture was purified via an HPLC system (Waters 600E, USA) on a Symmetry 300 Å C-4 reverse-phase column (250 mm × 10.0 mm, Sepax Bio.) using a solvent gradient. The mobile phase A consisted of distilled H_2O with 0.1% (v/v) trifluoroacetic acid (TFA), and mobile B of acetonitrile with 0.1% (v/v) TFA. The elution gradient was a 60 min linear gradient from 70% B to 90% B at a flow rate of 3 mL/min. L-SP5-PEG-DSPE was synthesized by the same procedure.

Preparation and Characterization of D-SP5-PEG-DSPE Micelles. *Preparation of Polymer Micelles.* Micelles loaded with Dox or DiR (tetramethylindotricarbocyanine, a near-infrared dye) were prepared, respectively, for different uses by the thin-film hydration and extrusion method. Nontargeted micelles loaded with Dox (M-micelles-Dox) were prepared by the follow procedures. First, 1 mg Dox·HCl was dissolved and stirred in 200 μL methanol at room temperature (molar ratio of Dox:triethylamine = 1:1.5) to convert into the Dox free base. After 8 h, the Dox methanol solution was transferred to a 500 μL $CHCl_3$ solution of 5 mg mPEG-DSPE. Next, the mixture was dried to form the drug-containing lipid film using a rotary evaporator, and vacuum was applied for complete removal of organic solvent. The obtained film was added to 200 μL 10 mM HEPES-buffered saline (HBS, pH 7.4), and then sonicated using a vortex shaker for 10 min. Then, the micelles were hydrated at 37 °C for 1.5 h. Free Dox was removed by gel filtration over a Sephadex G-50 column with HBS.

The formulations of D-SP5-micelles-Dox and L-SP5-micelles-Dox were prepared as described above except that 2 mol % of D-SP5-PEG-DSPE or L-SP5-PEG-DSPE (molar ratio of peptide-PEG-DSPE:mPEG-DSPE = 2:100) were added in the film preparation step. DiR-loaded micelles were prepared analogously except that DiR was dissolved in the $CHCl_3$/MeOH solution. All the procedures were conducted in darkness.

Particle Size and Dox Loading Efficiency of Polymer Micelles. Average diameters and size distribution of prepared micelles were determined by dynamic light scattering (DLS) method (Malvern Zetasizer 3000). Morphology of micelles was characterized by cryogenic transmission electron microscopy (cryo-TEM). One drop of Dox-loaded micelle solution was placed on a copper grid and was prepared as a thin aqueous film supported on a holey carbon grid. The grid was allowed to dry further for 10 min and was then examined with the electron microscope. Cryo-TEM images were obtained with a 200 kV Tecnai F20 (FEI, Netherlands).

To calculate drug loading efficiency, 900 μL acid isopropyl alcohol (volume ratio of concentrated HCl:ispropyl alcohol = 1:9) was added to 100 μL freshly prepared micelles (in HBS solution), to cause complete dissolution of the micelles and release of encapsulated Dox. The amount of loaded Dox was determined by measuring the UV absorbance at 483 nm. A calibration curve was constructed using different concentrations of free Dox (1−50 μg/mL) in an identical solvent mixture. The

dx.doi.org/10.1021/bc300537z | *Bioconjugate Chem.* 2013, 24, 133−143

level of Dox-loading and encapsulation efficiency were calculated from the following equations:

$$\text{Dox-loading[weight/weight](\%)} = (\text{amount of loaded Dox in mg}) / (\text{amount of copolymer in mg}) \times 100$$

$$\text{Encapsulation efficiency(\%)} = (\text{amount of loaded Dox in mg}) / (\text{amount of Dox added in mg}) \times 100$$

Release of Dox from Polymeric Micelles. The release profile of Dox from micelles was studied within 48 h, using the dialysis method. A 1.0 mL solution of free Dox, M-micelles/Dox, L-SP5-micelles/Dox, or D-SP5-micelles/Dox at the Dox concentration of 0.25 mg/mL was placed in a dialysis bag (molecular mass cutoff 10 kDa). The dialysis bags were incubated in 200 mL of either phosphate buffer (pH 7.4) or acetate buffer (pH 5.0) at 37 °C with gentle shaking, and aliquots were removed from the medium at defined time points. The released drug was quantified by fluorescence detection using reverse-phase HPLC (C18 column, 35% acetonitrile as the eluant solution).

Tumor Targeting Ability of D-SP5-Micelles. Mice bearing KB xenograft tumors were established by subcutaneous injection of 1.2×10^6 KB cells into the right flank. When the tumors reached 700 mm^3 after 3 weeks, D-SP5-micelles/DiR were injected via the tail vein, and L-SP5-micelles/DiR and M-micelles/DiR were used as control. At defined times post-injection, the mice were anesthetized and detected in the whole body using an in vivo imaging system (Maestro, CRI, USA) equipped with Deep Red filter sets (excitation/emission, 730/790 nm). After the time point of 24 h, mice were sacrificed by cervical dislocation, organs and tumors were harvested, and the distribution of fluorescence was calculated.

Pharmacodynamic Studies of D-SP5-Micelles/Dox. *MTT Cell Viability Assay.* The cytotoxicity of Dox-incorporated micelles against KB cells was determined by using 96-well tissue culture plates (Power Wave XS, Bio-TEK, USA). KB cells were seeded in 96-well plates in 200 μL of medium to obtain a concentration of 3000 cells per well and incubated overnight. Cells were then incubated with fresh, serum-free DMEM medium containing D-SP5-micelles/Dox, L-SP5-micelles/Dox, M-micelles/Dox, and free Dox with a series of Dox concentrations ranging from 0.85 μM to 54.50 μM for 2 h. Cells were washed with PBS twice, and 200 μL DMEM (containing 10% FBS) was added to each well and incubated for another 48 h. Then, 20 μL MTT was added to each well. After a further incubation period of 4 h, the absorbance was measured at 490 nm using an automatic multiwell spectrophotometer. Untreated cells in media were used as a control. The viability was calculated on the basis of absorbance of the study group over the control group. All experiments were carried out three times.

Effect of D-SP5-Micelles/Dox on KB Tumor Growth. Thirty four-week-old (18−20g) male BALB/C nude mice were injected subcutaneously in the right flank with 1.2×10^6 KB cells to establish xenograft tumors. After 14 days, the tumor volume had reached 100 mm^3; mice bearing KB tumors were randomized into five groups (six mice every group) and received intravenous (i.v.) injections of D-SP5-micelles/Dox, L-SP5-micelles/Dox, M-micelles/Dox, free Dox, and PBS (control group), separately, with a total doxorubicin dose of 10 mg/kg (five times, equivalent to 60 μg Dox/mouse/time) once each at the 14th, 17th, 20th, 23rd, and 26th day. The tumor volume was measured three times a week using the formula 0.5 ($a \times b^2$), where a and b refer to the largest and smallest diameter, respectively. After 21 days of treatment (the 34th day in total), mice were sacrificed by cervical dislocation, and the tumors were harvested and then weighed.

Systemic Toxicity of Micelle-Encapsulated Dox. Doxorubicin treatment results in severe irreversible cardiomyopathy. Therefore, we compared the systemic toxicity of free Dox with D-SP5-micelles/Dox, L-SP5-micelles/Dox, and M-micelles/Dox. To evaluate the tissue damage of different formulations, hearts were also collected after the mice were killed on day 34. Sections of 10 μm thickness were made, and H&E staining was performed, followed by pathological examination to identify the heart tissue damage.

Statistical Analysis. All the data are means ± SD calculated from at least three independent experiments. All of the paired data were tested for normality and considered Gaussian, so data sets were compared using the paired t test. The level of significance was set to $p < 0.05$.

RESULTS

FITC-D-SP5 Showed Dual Specific and Stronger Binding Efficacy to VEGF-Stimulated HUVEC Cells and Tumor Cells than FITC-L-SP5. In order to investigate the cellular uptake of D-SP5 to human neovasculature endothelium, FITC-labeled D-SP5 (FITC-D-SP5) and L-SP5 (FITC-L-SP5) were incubated with VEGF-stimulated HUVEC. As shown in Figure 1A(a,b), the FITC-D-SP5 showed enhanced cellular uptake by the VEGF-stimulated HUVEC compared to the FITC-L-SP5. No binding activity was observed for control peptide group (Figure 1A(c)). Most importantly, L-SP5 could completely inhibit the uptake of FITC-D-SP5 by stimulated-HUVEC (Figure 1A(d)). No fluorescent signal was observed in the case of HUVEC without VEGF stimulation (Figure 1A(e)). These results demonstrated that D-SP5 has a stronger targeting ability to the VEGF-stimulated HUVEC in comparison to L-SP5. In addition, it shows that the retro-inverso D-SP5 peptide was bound to the same binding site as the L-SP5.

To demonstrate the interaction of the D-SP5 with tumor cells in vitro, we incubated FITC-labeled D-SP5 and L-SP5 with three human tumor cells (i.e., KB, U87, and SGC), respectively. The D-SP5 showed more efficient internalization by KB cells than the L-SP5 (Figure 1B(a,b)). The control peptide did not show cellular uptake by KB (Figure 1B(c)). We also investigated other tumor cells such as U87 and SGC cells. The same results were obtained (Figure 1B(d,e;g,h)). The D-SP5 did not show cellular uptake of normal human hepatocyte cells (Figure 1B(f)). These results confirmed that the D-SP5 could target tumor cells better than the L-SP5.

^{125}I Iodinated D-SP5 Peptide Exhibited Higher Binding Affinities and More Binding Capacities to the Target Cells. To investigate the binding activity quantitatively, radioreceptor binding assays of ^{125}I-D-SP5 and ^{125}I-L-SP5 on the cells were performed. Briefly, 1×10^6 cells were incubated with increasing concentrations (0.01−1.5 nmol/L) of the ^{125}I-D-SP5 and ^{125}I-L-SP5. Saturation curves and Scatchard plots of specific binding of the ^{125}I-D-SP5 and ^{125}I-L-SP5 to the VEGF-stimulated HUVECs and three human tumor cells lines are presented in Figure 2. Scatchard analysis revealed a single class of high-affinity D-SP5 binding sites in VEGF-stimulated

dx.doi.org/10.1021/bc300537z | Bioconjugate Chem. 2013, 24, 133−143

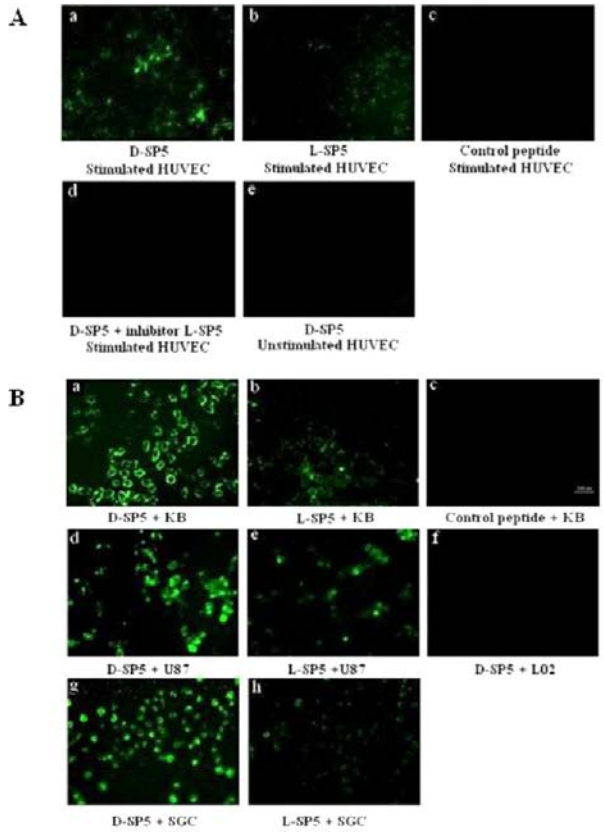

Figure 1. In vitro binding property of D-SP5 to VEGF-stimulated HUVECs and tumor cells. (A) The cellular uptake of D-SP5 by stimulated HUVECs: (a) D-SP5 with stimulated HUVECs; (b) L-SP5 with stimulated HUVECs; (c) control peptide with stimulated HUVECs; (d) D-SP5 inhibited by L-SP5 with stimulated HUVECs; (e) D-SP5 with unstimulated HUVECs. (B) The cellular uptake of D-SP5 by tumor cells: (a,d,g) D-SP5 and (b,e,h) L-SP5 with three different tumor cell lines; (c) control peptide with KB cells; (f) D-SP5 with L02 cells.

HUVEC and three human tumor cell lines (Table 2). ^{125}I-D-SP5 bound to stimulated HUVEC, KB, U87, and SGC with K_d of 131, 588, 769, and 2000 pmol/L, while L-SP5 bound to the cells with K_d of 232, 1250, 833, and 2500 pmol/L. Maximum binding capacity (B_{max}) of D-SP5 to the stimulated-HUVEC, KB, U87, and SGC were 61, 243, 137, and 164 fmol per 10^6 cells and those of L-SP5 were 24, 160, 38, and 115 fmol per 10^6 cells. In comparison with L-SP5, D-SP5 showed higher affinity and more apparent binding capacity with all the cells studied. Moreover, no specific binding of ^{125}I-labeled D-SP5 and L-SP5 to normal human hepatocyte cells (HL7902) was observed.

FITC Labeled D-SP5 Peptide Homes to Tumor Vessels of Mice Bearing KB Xenograft Tumors. Frozen tumor tissue sections were subjected to immunofluorescence analysis to study the localization of D-SP5 targeted to the KB tumor. The staining results of tumor tissues are shown in Figure 3. FITC-labeled D-SP5 completely colocalized with tumor blood vessel marker CD31. L-SP5 showed surprisingly lower colocalization with CD31. This, however, is consistent with the lower K_d and instability of L-SP5 in mouse serum (Figure 4). In sum, the data indicate more tumor neovasculature-specific binding of D-SP5 peptide.

D-SP5 Peptide Showed Sustained Serum Stability Compared with L-SP5 Peptide. Stability is considered as another important factor, because if the peptides were not stable in body fluids, they would fail to reach the tumor target sites. As shown in Figure 4, L-SP5 peptide was decomposed at an amazing rate, and within 1 h, L-SP5 was fully degraded in the serum; while D-SP5 peptide showed remarkably enzyme-resistant ability, for after 10 h, the remaining amount of D-SP5 was as much as 93%.

Synthesis and Characterization of D-SP5-PEG-DSPE. For formation of tumor-targeted micelles, peptide-PEG-DSPE conjugates (structures shown in Supporting Information Figure S2) were synthesized as described in Materials and Methods. In the ^{1}H NMR spectrum (Figure S2) of Mal-PEG-DSPE, the multiple peaks at 1.26 ppm refer to the methylene protons of DSPE, the signal at 3.7−3.8 ppm to the repeat units of PEG, and the characteristic peak at 6.7 ppm refers to the Mal group. This Mal peak is not present in the NMR spectra of D-SP5-PEG-DSPE and L-SP5-PEG-DSPE, whereas the DSPE and PEG segments still presented peaks at 1.26 and 3.7−3.8 ppm, respectively, indicating that the Mal group had reacted with the thiol group of D-SP5-cys and L-SP5-cys.

Physicochemical Properties of Dox-Loaded Micelles. The characterization results and transmission electron microscope (TEM) images are shown in Table 3 and Figure 5A. The size of micelles is about 30 nm and similar with or without D-SP5 or L-SP5 modification, demonstrating that the incorporation of D-SP5-PEG-DSPE or L-SP5-PEG-DSPE into micelles had no influence on the physical properties of micelles.

A time course of Dox release from micelles at 37 °C and either pH 7.4 or pH 5.0 was performed using a dialysis membrane assay for collection of released Dox. Most (85%) of free Dox was released from the dialysis bag within 2 h at pH 5.0 (Figure 5B), while the release of free Dox at pH 7.4 (Figure 5C) was slower (47% at the 2 h time point). At pH 5, nontargeted M-micelles/Dox, targeted L-SP5-micelles/Dox, and D-SP5-micelles/Dox released 18%, 18%, and 16% of encapsulated Dox after 24 h, respectively. Similar to that for free Dox, Dox release from polymeric micelles was slower at pH 7.4 compared to pH 5.0. At pH 7.4, 13.5%, 13.2%, and 10.3% of encapsulated Dox were released from M-micelles/Dox, L-SP5-micelles/Dox, and D-SP5-micelles/Dox after 24 h, respectively.

D-SP5-Micelles Delivery Resulted in Enhanced Tumor Targeting. The in vivo targeting property of D-SP5-micelles to KB xenograft tumors was based on the study by injecting micelles loaded with DiR via tail vein to nude mice bearing tumors. As is shown in Figure 6A, for each time point at 1, 4, and 8 h, significantly increased fluorescence was observed in the tumor site of D-SP5-micelles, suggesting that more D-SP5-micelles-DiR localized in the tumor site than L-SP5-micelles-DiR and M-micelles-DiR groups. According to the image of in vitro excised organs shown in Figure 6B, tumor and liver showed obvious fluorescence, while limited accumulation was observed in heart. A triple increase of fluorescence of D-SP5-micelles (semiquantitative analysis) in tumor but not heart suggests that D-SP5-micelles-DiR might have improved antitumor efficiency and decreased cardiac toxicity (Figure 6C).

Enhanced Tumor Growth Inhibition by D-SP5-Micelles/Dox. Dose-dependent in vitro cytotoxicity of D-SP5-micelles/Dox, L-SP5-micelles/Dox, M-micelles/Dox, and free Dox was demonstrated on KB tumor cells by MTT assay as shown in Figure 7A. The unloaded control micelles showed no noticeable cell death up to 1000 mg/L (Figure 7B), indicating their good biocompatibilities and displaying their potential as drug delivery vehicles. Effective inhibitory effect of KB cells was

dx.doi.org/10.1021/bc300537z | Bioconjugate Chem. 2013, 24, 133−143

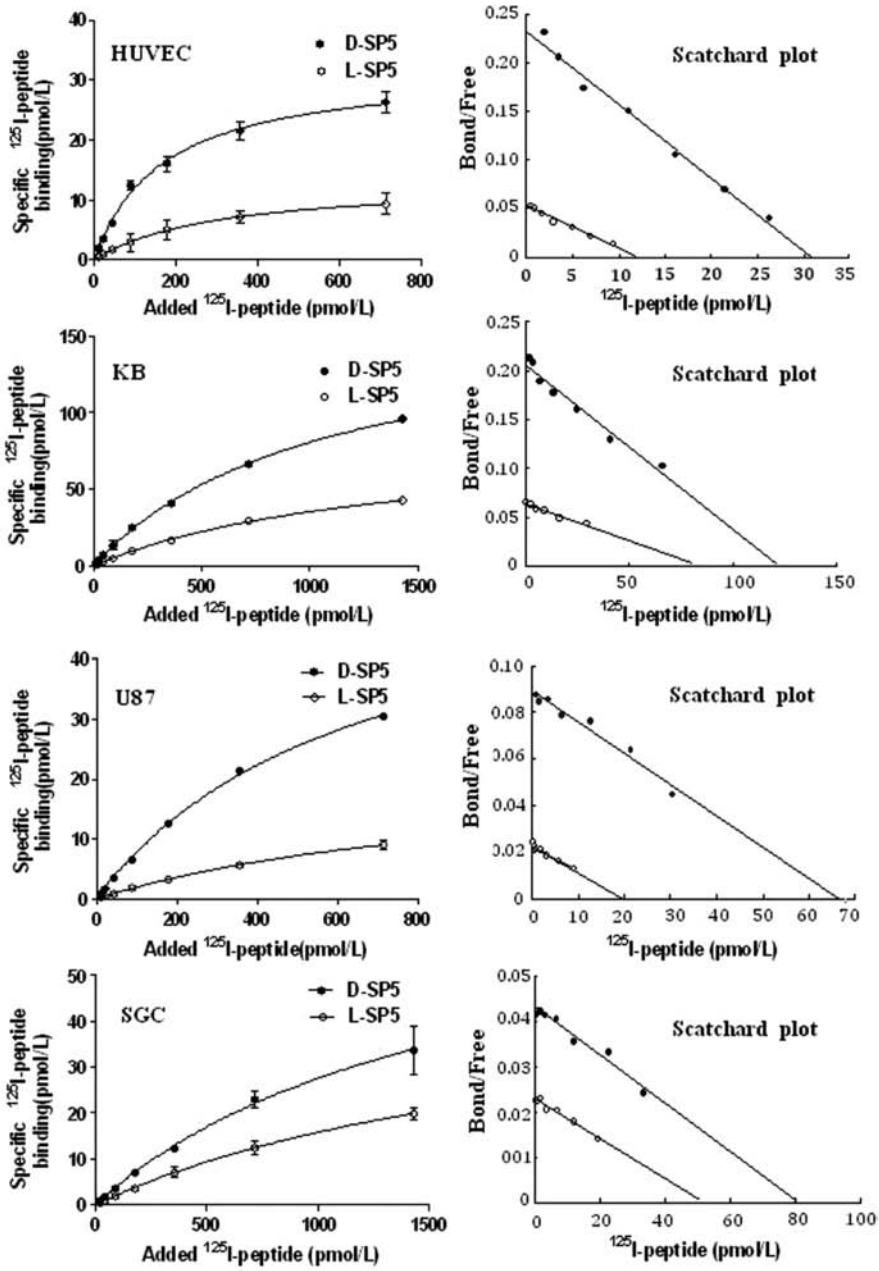

Figure 2. Radio receptor binding assays on the cells using ^{125}I-labeled peptides (---●---, D-SP5; ---○---, L-SP5). Specific binding was calculated from total binding by subtracting nonspecific binding. Nonspecific binding was determined experimentally in the presence of no less than a 200 molar excess of unlabeled peptide. The binding reaction proceeded for 4 h at 4 °C. Data from three experiments performed in triplicate are shown.

found in both groups. Modified with D-SP5, the half maximal inhibitory concentration (IC_{50}) was 1.69 μM, while IC_{50} values for free Dox, M-micelles/Dox, and L-SP5-micelles/Dox being 4.36 μM, 7.94 μM, and 2.91 μM, respectively, which were significantly higher than D-SP5-micelles/Dox ($p < 0.001$). These results indicated that D-SP5-micelles/Dox are more efficient to mediate cytotoxicity of Dox than other formulations.

Improved Retardation of Tumor Growth by Intravenous D-SP5-Micelles/Dox Delivery. The inhibition effect of D-SP5-micelles/Dox against KB xenograft tumor nude mice was shown in Figure 8. We found that the tumor volumes of the D-SP5-micelles/Dox group were significantly smaller than those of free Dox, L-SP5-micelles/Dox, and M-micelles/Dox in the whole measuring period ($p < 0.05$, compared to the three other groups). After the mice were sacrificed, xenografted tumors were excised and weighed. There was no significant difference in average tumor weights among free Dox, micelles/Dox, and L-SP5-micelles/Dox, while D-SP5-micelles/Dox showed the superior tumor-suppression effect compared to L-SP5-micelles/Dox ($P < 0.01$, Figure 8B). All these results indicated that D-SP5-micelles/Dox serves as a better treatment vehicle compared to L-SP5-micelles/Dox. The body weights of each group showed no significant changes (data not shown).

No Significant Heart Toxicity of D-SP5-Micelles/Dox. H&E staining results for hearts of the mice treated with Dox loaded micelles and free Dox are shown in Figure 9. The muscle fibers of free Dox goup mice showed obvious damage, for the obviously loss of striation and fiber fragmentation (Figure 9A). Histopathological changes in cardiac tissues from mice treated with D-SP5-micelles/Dox, L-SP5-micelles/Dox,

dx.doi.org/10.1021/bc300537z | Bioconjugate Chem. 2013, 24, 133−143

Table 2. K_ds and B_{max} of the D-SP5 and L-SP5 to Different Cell Lines

cell lines		peptides	B_{max} (fmol/ 10^6 cell)	K_d (pmol/ L)	R^2
HUVEC	human umbilical vein endothelial cells	D-SP5	61	131	0.9806
		L-SP5	24	232	0.9864
KB	human oral epidermoid carcinoma	D-SP5	243	588	0.9621
		L-SP5	160	1250	0.9697
U87	human brain glioblastoma	D-SP5	137	769	0.9646
		L-SP5	38	833	0.9658
SGC	human gastric carcinoma	D-SP5	164	2000	0.9633
		L-SP5	115	2500	0.9708
L02	normal human hepatocyte	D-SP5	----	----	----
		L-SP5	----	----	----

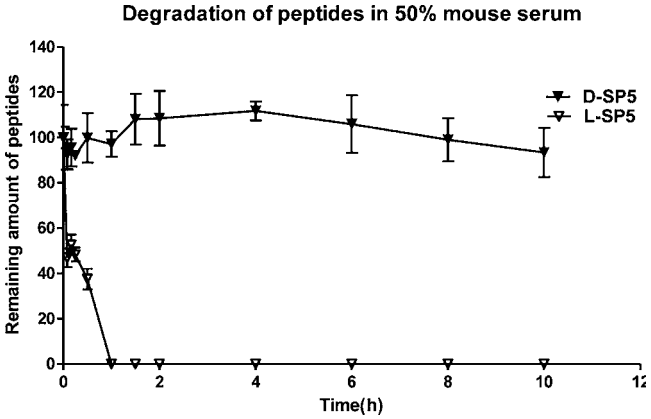

Figure 4. Degradation of D-SP5 and L-SP5 peptides in 50% mouse serum. The peptides were incubated with 50% mouse serum at 37 °C for different time periods, and the remaining peptide amounts were determined by HPLC.

Table 3. Characteristics of Dox-Loaded Polymeric Micelles (n = 3)

formulation	average micellar size ± SD (nm)	polydispersity index (PDI)
M-micelles/Dox	30.4 ± 2.8	0.299
D-SP5-micelles/ Dox	31.2 ± 2.0	0.312
L-SP5-micelles/ Dox	33.1 ± 2.6	0.287

and M-micelles/Dox showed little signs of toxicity to muscle fibers (Figure 9B,C,E). No differences compared with the normal muscle fibers from mice receiving PBS (Figure 9D) were observed.

DISCUSSION

Cancer chemotherapy is frequently accompanied by strong side effects and acquired drug resistance. Therefore, the most important goal of current anticancer research is to deliver drugs to the proper target sites. Phage display is a powerful tool for identifying novel peptides with high specificity to a desired target tissue such as tumor cells or tumor blood vessels.[31,32] Among these homing peptides, L-SP5 was discovered by in vivo phage display as a linear sequence that efficiently and specially binds to tumor blood vasculature. [29] Its specific target is not yet known, but a proline-serine-proline motif within the peptide sequence was found to be essential for neovasculature binding.

Possible weaknesses of phage-derived targeting sequence include degradability of peptides by proteases and inherent antigenicity of these artificial sequences. In the current study, we utilize the retro-inverso strategy for further optimization of bioactivity of the SP5 targeting peptide. According to the retro-inverso strategy,[33−35] for nonhelical sequences the replacement of L- by D-amino acids (which generates a perfect mirror-image of the peptide) in combination with reversing the amino acid sequence so that the N-terminal residue appears as C-terminal residue and vice versa (which generates a pseudo mirror image), this double mirroring process generates a *retro-inverso* peptide with very similar side chain orientation as in the original L-peptide. Despite the fact that phage display technology has been widely used in seeking for tumor-targeting peptides, no related investigation has been found to have applied the retro-inverso concept to improve their bioactivity. In our study, we used this strategy for design of the retro-inverso form of L-SP5 ($_L$(SVSVGMKPSPRP)), named D-SP5 ($_D$(PRPSPKMGVSVS)). Simultaneously, cysteine and tyrosine derivatives of D-SP5 were also synthesized for further modification, and cysteine or tyrosine was conjugated to the C terminus of D-SP5

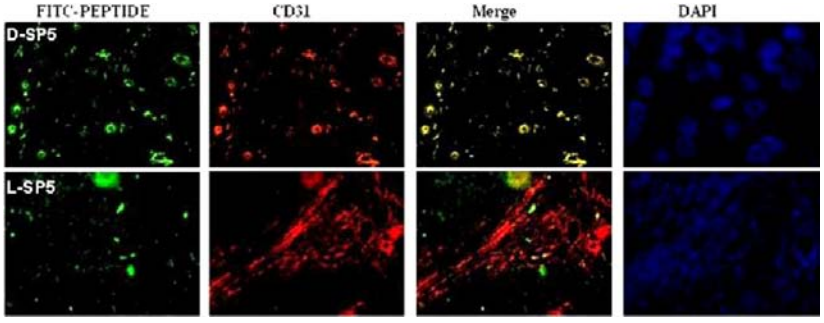

Figure 3. Immunofluorescence colocalization of D-SP5 peptide and CD31 in the tumor tissues of nude mice bearing KB tumors. Mice bearing KB xenograft tumors were intravenously injected with FITC-labeled D-SP5 and L-SP5 (green). The mice were sacrificed 2 h later and tumor tissues were excised and cut into slices. The sections were counterstained with CD31 antibody (red) for tumor blood vessel and DAPI (blue) was used for nuclei staining. The merged images showed yellow color areas by overlaying images of the counterstaining. Upper layer: D-SP5 completely colocalized with the CD31. Lower layer: L-SP5 colocalized less with the CD31 endothelial marker.

dx.doi.org/10.1021/bc300537z | *Bioconjugate Chem.* 2013, 24, 133−143

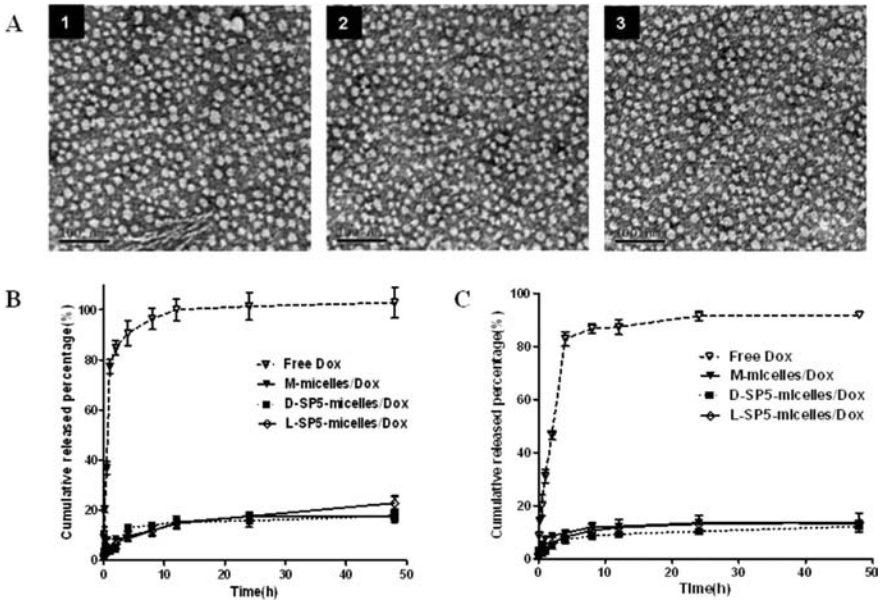

Figure 5. Physicochemical properties of Dox loaded micelles. (A) Transmission electron microscope images of micelles: 1, M-micelles/Dox; 2, L-SP5-micelles/Dox; 3, D-SP5-micelles/Dox. Time course of Dox release from micelles at 37 °C at pH 5.0 (B) or pH 7.4 (C). Released Dox was separated from micelle-embedded Dox by dialysis and quantified fluorimetrically using HPLC.

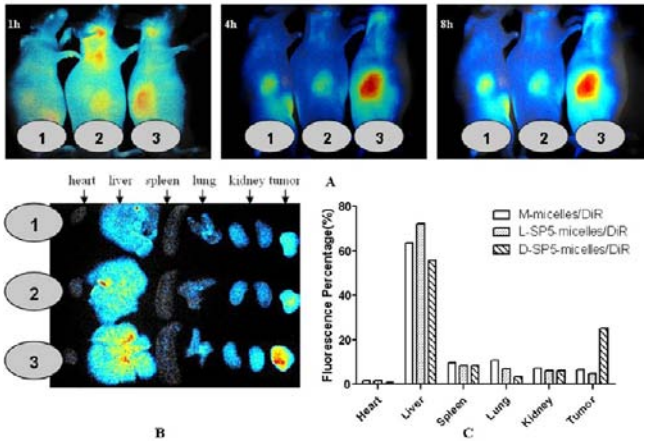

Figure 6. Fluorescent images of M-micelles/DiR, L-SP5-micelles/DiR, and D-SP5-micelles/DiR on KB xenograft tumor-bearing mice after injection via tail vein. (A) In vivo imaging at 1, 4, and 8 h: 1, mice injected with M-micelles/DiR; 2, mice injected with L-SP5-micelles/DiR; 3, mice injected with D-SP5-micelles/DiR. (B) Imaging on ex vivo tissues of KB xenograft tumor-bearing mice 24 h after injection via tail vein. (C) Semiquantitative analysis of organs for different groups of mice (M-micelles/DiR; L-SP5-micelles/DiR; D-SP5-micelles/DiR).

that was far away from the crucial PSP motif sequence.[29] FITC-labeled D-SP5 peptide was internalized by HUVECs with but not without VEGF stimulation. In addition, the radioreceptor binding test showed the ^{125}I-labeled D-SP5 specially bound to VEGF-stimulated HUVEC with higher binding affinity and abundant binding sites (K_d values of 131 pmol/L and B_{max} values of 61 fmol/10^6 cell, compared with 232 pmol/L and 24 fmol per 10^6 cells for L-SP5). Several target receptors, such as the vascular endothelial growth factor receptor (VEGFR) or other growth factor receptor, are expressed not only on the tumor endothelial cells, but also on a variety of tumor cells.[36−39] Accordingly, we also investigated the binding activity of D-SP5 to several tumor cell lines. The results demonstrated that D-SP5 peptide also has high affinity to human oral epidermoid carcinoma (KB), human brain glioblastoma (U87), and human gastric carcinoma (SGC). This indicates that D-SP5 peptide could target both tumor vessels and tumor cells. The similar spacial position of the amino acid side of the retro-inverso D-SP5 peptide as in the original L-SP5 peptide explains the bioactivity retained. However, the side chain orientation is not identical in the D-SP5 peptide compared to the L-SP5. Therefore, and also because the receptor is not known, it was not predictable whether the D-SP5 is more suitable to bind with the cellular receptors or not.

Interestingly, according to our study D-SP5 peptide exhibited a stronger affinity and more binding capacity in human stimulated HUVEC and tumor cells in comparison with L-SP5. With the modification of D-SP5, intravenously applied PEG-DSPE micelles demonstrated an at least 3-fold higher tumor accumulation (near-infrared bioimaging, Figure 6) and, when loaded with Dox, showed a markedly stronger tumor inhibition efficiency compared with L-SP5 micelles/Dox, M-micelles/Dox, and free Dox (Figure 8). Studies showed that D-SP5-micelles/Dox formulation also enhanced the in vitro cytotoxicity of Dox against KB cells (Figure 7A). The nontargeted polymeric micelles of Dox did not show significantly improved antitumor effects, neither in vitro nor in vivo, but nevertheless, the nanoformulation reduced the side effects of Dox-induced cardiac myopathy (Figure 9) This lack of toxicity due to absence of high dose of free Dox is consistent with the finding that less than 20% Dox encapsulated in the micelles was released in 48 h in an in vitro assay (Figure 5B,C). Most importantly, the D-SP5 targeted micelle formulation of Dox also displayed no detectable cardiac toxicity (Figure 9).

CONCLUSIONS

In summary, we designed the retro-inverso peptide D-SP5, $_D$(PRPSPKMGVSVS), with potent dual-targeting to tumor neovasculature and tumor cells. D-SP5 and the parental L-SP5 utilize the same binding site (a currently still unknown receptor). The D-SP5 peptide has significantly increased

dx.doi.org/10.1021/bc300537z | Bioconjugate Chem. 2013, 24, 133−143

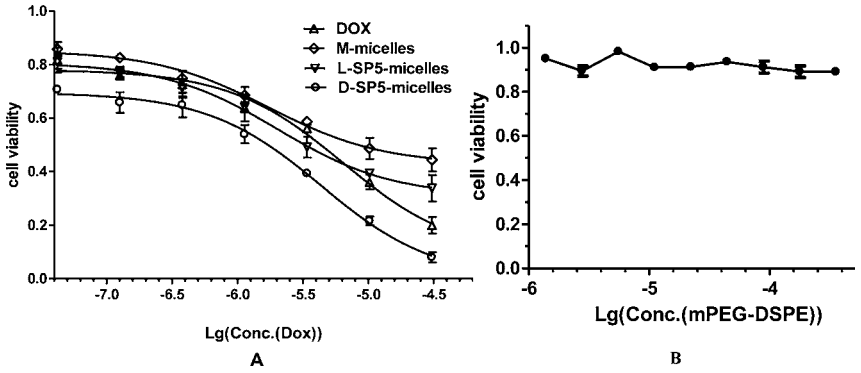

Figure 7. Antitumoral efficacy of Dox loaded micelles on KB cells in vitro. (A) Growth inhibition of KB tumor cell growth by Dox loaded micelles (D-SP5-micelles/Dox L-SP5-micelles/Dox, and M-micelles/Dox) and free Dox, as determined by MTT assay. The IC_{50} values for D-SP5-micelles/Dox, L-SP5-micelles/Dox, M-micelles/Dox, and free Dox were 1.69, 2.91, 7.94, and 4.36 μM, respectively. (B) Cytotoxicity of nonloaded mPEG-DSPE micelles.

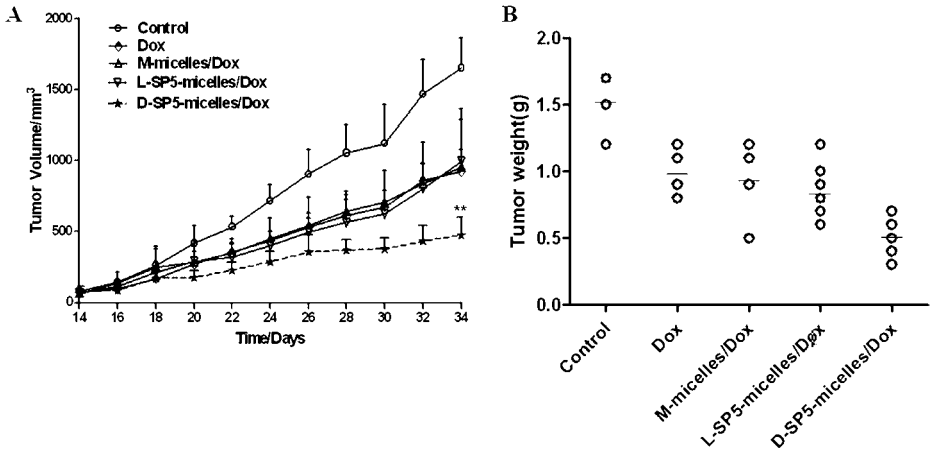

Figure 8. Response of SCID mice bearing KB xenografts to intravenous administration of D-SP5-micelles/Dox. (A) The growth of tumor sizes of D-SP5-micelles/Dox group is markedly suppressed compared with L-SP5-micelles/Dox, M-micelles/Dox, and free Dox groups. (n = 6; **, P < 0.01). (B) Tumor weight of each group after 21 days of treatment.

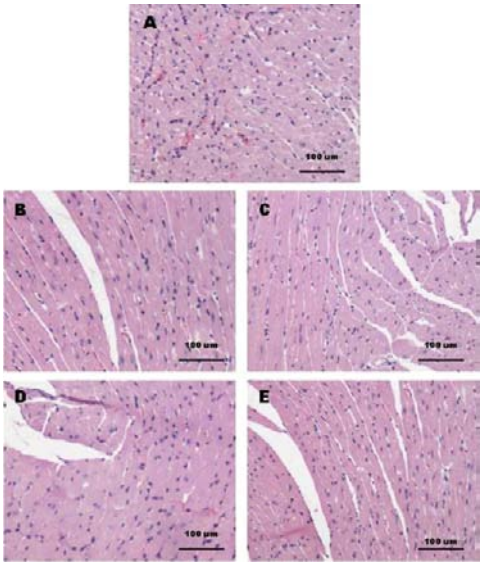

Figure 9. Lack of cardiac toxicity of micelles/Dox formulations. H&E staining of hearts of KB xenograft tumor-bearing nude mice treated with different formulations (A, free Dox; B, D-SP5-micelles/Dox; C, L-SP5-micelles; D, control; E, M-micelles/Dox).

binding affinity and also higher binding capacity as compared with the parental L-SP5 peptide. Targeting micelles via D-SP5 peptide enhanced tumor homing and, when loaded with Dox, inhibited the tumor growth, resulting in increased therapeutic efficacy in KB xenograft mice. Therefore, D-SP5 is an effective agent for drug delivery to both tumor vessels and some specific tumor cells and may be a potential targeting vehicle for application in clinical cancer treatment.

■ ASSOCIATED CONTENT

Ⓢ Supporting Information

Additional data of peptides, MS spectra and chemical structures, and ^{1}H-NMR spectra. This material is available free of charge via the Internet at http://pubs.acs.org.

■ AUTHOR INFORMATION

Corresponding Author

*Tel.: +86 21 51980092. Fax: + 86 21 51980090. E-mail: liumin@shmu.edu.cn.

Notes

The authors declare no competing financial interest.

■ ACKNOWLEDGMENTS

This work was supported by National Key Basic Research Program of China (No. 2013CB932502), and National Science

Foundation of China (No. 30772655 and No .81001200). Dr. Ernst Wagner is a professor at Ludwig-Maximilians-Universität (LMU) Munich, Germany. As a visiting professor at Fudan University, he appreciates receiving a Fudan University Key Laboratory Senior Visiting Scholarship.

REFERENCES

(1) Bosslet, K., Straub, R., Blumrich, M., Czech, J., Gerken, M., Sperker, B., Kroemer, H. K., Gesson, J. P., Koch, M., and Monneret, C. (1998) Elucidation of the mechanism enabling tumor selective prodrug monotherapy. *Cancer Res. 58*, 1195−1201.

(2) Chang, D. K., Lin, C. T., Wu, C. H., and Wu, H. C. (2009) A novel peptide enhances therapeutic efficacy of liposomal anti-cancer drugs in mice models of human lung cancer. *PLoS One 4*, e4171.

(3) Jain, R. K. (1987) Transport of molecules in the tumor interstitium: a review. *Cancer Res. 47*, 3039−3051.

(4) Heldin, C. H., Rubin, K., Pietras, K., and Ostman, A. (2004) High interstitial fluid pressure - an obstacle in cancer therapy. *Nat. Rev. Cancer 4*, 806−813.

(5) Lunt, S. J., Kalliomaki, T. M., Brown, A., Yang, V. X., Milosevic, M., and Hill, R. P. (2008) Interstitial fluid pressure, vascularity and metastasis in ectopic, orthotopic and spontaneous tumours. *BMC Cancer. 7* (8), 2.

(6) Maeda, H., Bharate, G. Y., and Daruwalla, J. (2009) Polymeric drugs for efficient tumor-targeted drug delivery based on EPR-effect. *Eur. J. Pharm. Biopharm. 71*, 409−419.

(7) Hashizume, H., Baluk, P., Morikawa, S., McLean, J. W., Thurston, G., Roberge, S., Jain, R. K., and McDonald, D. M. (2000) Openings between defective endothelial cells explain tumor vessel leakiness. *Am. J. Pathol. 156*, 1363−1380.

(8) Drummond, D. C., Meyer, O., Hong, K., Kirpotin, D. B., and Papahadjopoulos, D. (1999) Optimizing liposomes for delivery of chemotherapeutic agents to solid tumors. *Pharmacol. Rev. 51*, 691−743.

(9) Kim, J. O., Kabanov, A. V., and Bronich, T. K. (2009) Polymer micelles with cross-linked polyanion core for delivery of a cationic drug doxorubicin. *J. Controlled Release 138*, 197−204.

(10) Mikhail, A. S., and Allen, C. (2009) Block copolymer micelles for delivery of cancer ther- py: transport at the whole body, tissue and cellular levels. *J. Controlled Release 138*, 214−223.

(11) Gaucher, G., Dufresne, M. H., Sant, V. P., Kang, N., Maysinger, D., and Leroux, J. C. (2005) Block copolymer micelles: preparation, characterization and application in drug delivery. *J. Controlled Release 109* (1−3), 169−188.

(12) Ruoslahti, E. (2004) Vascular zip codes in angiogenesis and metastasis. *Biochem. Soc. Trans. 32*, 397−402.

(13) Rafii, S., Avecilla, S. T., and Jin, D. K. (2003) Tumor vasculature address book:indentifi- cation of stage-specific tumor vessel zip codes by phage display. *Cancer Cell 4* (5), 331−333.

(14) Thorpe, P. E., and Ran, S. (2002) Mapping zip codes in human vasculature. *Pharmacogenomics J. 2*, 205−206.

(15) Rajotte, D., Arap, W., Hagedorn, M., Koivunen, E., Pasqualini, R., and Ruoslahti, E. (1998) Molecular heterogeneity of the vascular endothelium revealed by in vivo phage display. *J. Clin. Invest. 102*, 430−437.

(16) Kolonin, M. G., Pasqualini, R., and Arap, W. (2001) Molecular addresses in blood vessels as targets for therapy. *Curr. Opin. Chem. Biol. 5*, 308−313.

(17) Drevs, J., and Schneider, V. (2006) The use of vascular biomarkers and imaging studies in the early clinical development of anti-tumour agents targeting angiogenesis. *J. Intern. Med. 260*, 517−529.

(18) Ruoslahti, E. (2002) Drug targeting to specific vascular sites. *Drug Discovery Today 7*, 1138−1143.

(19) Lee, T. Y., Wu, H. A. N. C., Tseng, Y. U. N. L., and Lin., C. T. (2004) A novel peptide specifically binding to nasopharyngeal carcinoma for targeted drug delivery. *Cancer Res. 64* (21), 8002−8008.

(20) Sapra, P., and Allen, T. M. (2002) Internalizing antibodies are necessary for improved therapeutic efficacy of antibody-targeted liposomal drugs. *Cancer Res. 62* (24), 7190−7194.

(21) Chang, D. K., Chiu, C. Y., Kuo, S. Y., Lin, W. C., Lo, A., Wang, Y. P., Li, P. C., and Wu, H. C. (2009) Antiangiogenic targeting liposomes increase therapeutic efficacy for solid tumors. *J. Biol. Chem. 284* (19), 12905−12916.

(22) Pastorino, F., Paolo, D. D., Piccardi, F., Nico, B., Ribatti, D., and Daga, A. (2008) Enhanc- ed antitumor efficacy of clinical-grade vasculature-targeted liposomal doxorubicin. *Clin. Cancer Res. 14*, 7320−7329.

(23) Sadowski, M., Pankiewicz, J., Scholtzova, H., Li, Y. S., Quartermain, D., Duff, K., and Wisniewski, T. (2004) Links between the pathology of Alzheimer's disease and vascular dementia. Neurochemical Research. *Neurochem. Res. 29* (6), 1257−1266.

(24) Goodman, M., and Chorev, M. (1979) Concept of linear modified retro-peptide structures. *Acc. Chem. Res. 12* (1), 1−7.

(25) Guichard, G., Benkirane, N., Zeder-Lutz, G., van Regenmortel, M. H., Briand, J. P., and Muller, S. (1994) Antigenic mimicry of natural L-peptides with retro-inverso-peptidomimetics. *Proc. Natl. Acad. Sci. U. S. A. 91*, 9765−9769.

(26) Cardó-Vila, M., Giordano, R. J., Sidman, R. L., Bronk, L. F., Fan, Z., and Mendelsohn, J. (2010) From combinatorial peptide selection to drug prototype (II): Targeting the epidermal growth factor receptor pathway. *Proc. Natl. Acad. Sci. U. S. A. 107* (11), 5118−5123.

(27) Briand, J. P., Guichard, G., Dumortier, H., and Muller, S. (1995) Retro-inverso peptidomimetics as new immunological probes-validation and application to the detection of antibodies in pheumatic diseases. *J. Biol. Chem. 270* (35), 20686−20691.

(28) Taylor, E. M., Otero, D. A., Banks, W. A., and O'Brien, J. S. (2000) Retro-inverso prosaptide peptides retain bioactivity, are stable in vivo, and are blood-brain barrier permeable. *J. Pharmacol. Exp. Ther. 295* (1), 190−194.

(29) Lee, T. Y., Lin, C. T., Kuo, S. Y., Chang, D. K., and Wu, H. C. (2007) Peptide-mediated targeting to tumor blood vessels of lung cancer for drug delivery. *Cancer Res. 67*, 10958−10965.

(30) Lin, C. M., Mihal, K. A., and Krueger, R. J. (1989) N-iodoacetyltyramine: preparation and use in 125I labeling by alkylation of sulfhydryl groups. *Anal. Biochem. 179* (2), 389−395.

(31) Ruoslahti, E. (2000) Targeting tumor vasculature with homing peptides from phage display. *Semin. Cancer Biol. 10*, 435−442.

(32) Teesalu, T., Sugahara, K. N., and Ruoslahti, E. (2012) Mapping of vascular ZIP codes by phage display. *Methods Enzymol. 503*, 35−56.

(33) Fischer, P. M. (2003) The design, synthesis and application of stereochemical and directional peptide isomers: a critical review. *Curr. Protein Pept. Sci. 4*, 339−356.

(34) Li, C., Pazgier, M., Li, J., Li, C., Liu, M., Zou, G., Li, Z., Chen, J., Tarasov, S. G., Lu, W. Y., and Lu, W. (2010) Limitations of peptide retro-inverso isomerization in molecular mimicry. *J. Biol. Chem. 285*, 19572−19581.

(35) Ruttekolk, I. R., Witsenburg, J. J., Glauner, H., Bovee-Geurts, P. H., Ferro, E. S., Verdurmen, W. P., and Brock, R. (2012) The intracellular pharmacokinetics of terminally capped peptides. *Mol. Pharm. 9*, 1077−1086.

(36) Reubi, J. C., Fleischmann, A., Waser, B., and Rehmann, R. (2011) Concomitant vascular GRP-receptor and VEGF-receptor expression in human tumors: molecular basis for dual targeting of tumoral vasculature. *Peptides 32*, 1457−1462.

(37) Guidi, A. J., Abu-Jawdeh, G., Tognazzi, K., Dvorak, H. F., and Brown, L. F. (1996) Expression of vascular permeability factor (vascular endothelial growth factor) and its receptors in endometrial carcinoma. *Cancer 78*, 454−460.

(38) Fleischmann, A., Waser, B., and Reubi, J. C. (2007) Overexpression of gastrin-releasing peptide receptors in tumor-associated blood vessels of human ovarian neoplasms. *Cell Oncol. 29*, 421−433.

(39) Smith, N. R., Baker, D., James, N. H., Ratcliffe, K., Jenkins, M., Ashton, S. E., Sproat, G., Swann, R., Gray, N., Ryan, A., Jürgensmeier, J. M., and Womack, C. (2010) Vascular endothelial growth factor

receptors VEGFR-2 and VEGFR-3 are localized primarily to the vasculature in human primary solid cancers. *Clin. Cancer Res. 16*, 3548−3561.

dx.doi.org/10.1021/bc300537z | *Bioconjugate Chem.* 2013, 24, 133−143